Radiation Medicine and Protection 1 (2020) 41–47

Contents lists available at ScienceDirect

Radiation Medicine and Protection

journal homepage: www.radmp.org

Motion robust 4D-MRI sorting based on anatomic feature matching: A digital phantom simulation study

Zi Yang [a], Lei Ren [a,b,**], Fang-Fang Yin [a,b], Xiao Liang [a], Jing Cai [b,c,*]

[a] Medical Physics Graduate Program, Duke University, Durham, NC, USA
[b] Department of Radiation Oncology, Duke University Medical Center, Durham, NC, USA
[c] Department of Health Technology and Informatics, The Hong Kong Polytechnic University, Kowloon, Hong Kong, China

ARTICLE INFO

Keywords:
Motion artifacts
4D-MRI
XCAT
Liver cancer
Simulation

ABSTRACT

Purpose: Motion artifacts induced by breathing variations are common in 4D-MRI images. This study aims to reduce the motion artifacts by developing a novel, robust 4D-MRI sorting method based on anatomic feature matching and applicable in both cine and sequential acquisition.

Method: The proposed method uses the diaphragm as the anatomic feature to guide the sorting of 4D-MRI images. Initially, both abdominal 2D sagittal cine MRI images and axial MRI images were acquired. The sagittal cine MRI images were divided into 10 phases as ground truth. Next, the phase of each axial MRI image is determined by matching its diaphragm position in the intersection plane to the ground truth cine MRI. Then, those matched phases axial images were sorted into 10-phase bins which were identical to the ground truth cine images. Finally, 10-phase 4D-MRI were reconstructed from these sorted axial images. The accuracy of reconstructed 4D-MRI data was evaluated by comparing with the ground truth using the 4D eXtended Cardiac Torso (XCAT) digital phantom. The effects of breathing signal, including both regular (cosine function) and irregular (patient data) in both axial cine and sequential scanning modes, on reconstruction accuracy were investigated by calculating total relative error (TRE) of the 4D volumes, Volume-Percent-Difference (VPD) and Center-of-Mass-Shift (COMS) of the estimated tumor volume, compared with the ground truth XCAT images.

Results: In both scanning modes, reconstructed 4D-MRI images matched well with ground truth with minimal motion artifacts. The averaged TRE of the 4D volume, VPD and COMS of the EOE phase in both scanning modes are 0.32%/1.20%/±0.05 mm for regular breathing, and 1.13%/4.26%/±0.21 mm for patient irregular breathing.

Conclusion: The preliminary evaluation results illustrated the feasibility of the robust 4D-MRI sorting method based on anatomic feature matching. This method provides improved image quality with reduced motion artifacts for both cine and sequential scanning modes.

1. Introduction

In radiation therapy, respiratory motion management is of significance, especially in the abdominal and thoracic cancers, where the organ and tumor motion is a major component of the treatment uncertainties. Four-dimensional (4D) imaging adds time as the fourth dimension into 3D volumetric images to introduce temporal information, especially the respiratory motion, into the spatial information. Generally, 4D imaging is generated by re-ordering and re-binning the data, whether reconstructed images or raw data, into pre-defined phase bins to reveal clear body respiratory motion during an entire breathing cycle without blurring in the motion path. Currently, the clinical standard of 4D imaging technique for radiation therapy is 4D Computed Tomography (CT). It is commonly used to evaluate and manage patient respiratory motion, especially for the lung and abdominal cancers.[1,2]

Recently, 4D Magnetic Resonance Imaging (MRI) has become an emerging technique for imaging respiratory motion.[3–12] 4D-MRI is a promising respiratory motion management modality with excellent soft-tissue contrast for tumor delineation with no known radiation hazard to the patients, compared with 4D-CT. A number of methods have been proposed for 4D-MRI development and have shown promising results for clinical applications. A detailed review of the 4D-MRI techniques can be found in the literature, and thus won't be detailed here.[13] In short, current 4D-MRI techniques are mostly based on retrospective sorting,

* Corresponding authors. Department of Health Technology and Informatics, The Hong Kong Polytechnic University, Kowloon, Hong Kong, China.
** Corresponding authors. Department of Radiation Oncology, Duke University Medical Center, Durham, NC, USA.
E-mail addresses: lei.ren@duke.edu (L. Ren), jing.cai@polyu.edu.hk (J. Cai).

https://doi.org/10.1016/j.radmp.2020.01.003

Available online 19 February 2020

either in image space for 2D acquisitions or in k-space for 3D image acquisitions. These 4D-MRI techniques often assume reproducible breathing patterns; thus, the sorting process will cause the motion artifact when breathing variation occurs, which presents as tissue discontinuities of the anatomic structures in the reconstructed 4D-MRI images in image-based sorting (2D acquisition) or as image blurring in k-space-based sorting (3D acquisition).

This study aims to develop a motion robust image-based 4D-MRI sorting method based on anatomic feature matching which can effectively reduce breathing variation induced motion artifacts. In this study, we developed an anatomic feature matching-based (AFM) 4D-MRI sorting method for both cine and sequential 2D MR acquisitions, and assessed the robustness of this method for irregular breathing using both simulated and patient breathing signals via a simulation study on a digital human phantom.

2. Methods & materials

2.1. The AFM 4D-MRI sorting method

2.1.1. Overall study design

Fig. 1 shows the overall workflow of the proposed AFM 4D-MRI sorting method. The general idea is to acquire two groups of orthogonal MRI images, then detect the anatomic features in the two image groups, and finally sort the images into different bins by matching their anatomic features to directly preserve better organ/tissue structure. In this method, we chose the diaphragm as the landmark feature to be detected and matched. The reasons for choosing the diaphragm are 1) tumor motion is primarily influenced by the diaphragm motion; 2) the respiratory motion is more dominant in the superior–inferior (SI) direction, which can be captured by the diaphragm; and 3) the diaphragm structure can be easily extracted from images due to the naturally defined border between liver and lung.

This detailed AFM 4D-MRI sorting method is described below in three steps:

(1) Image acquisition: Two groups of orthogonal scans are acquired in this process. The first group is the single-slice sagittal cine images located at the right diaphragm peak location (where the diaphragm is most superior). They are acquired over several breathing cycles. The second group is the axial slices located at multiple positons acquired over a volume of interest, which is the 4D-MR scan. The acquisition mode of this axial scan can be either cine mode or sequential mode.

(2) Diaphragm Extraction: The second step is to detect the diaphragm in those two groups of images. For the sagittal single-slice cine images, 10 reference images representing 10 respiratory phase bins in a breathing cycle are first selected according to the diaphragm motion in the images. Then the diaphragm structures in these 10 sagittal images are extracted by a region-growing based method as shown in Fig. 2[14] Note that, to improve the detection accuracy, the diaphragm is identified with two steps. This extraction method consists of the following sub-steps: (a) manual selection of a seed point inside the liver region in the sagittal image and selection of a 9-by-9 pixel matrix around the seed point; (b) calculation of the image intensity threshold of the liver by averaging the 3 maximum intensity values and 3 minimum intensity values in the matrix to reduce the influence of noise and filtering of the image intensity using this threshold to be within the liver intensity range; (c) using the region-growing algorithm to extract the liver boundary by searching image pixels within the threshold starting from the seed point; (d) using Otsu's method to change the image into a binary format.[15] This method will change the body intensity into 1 and change the lung and background intensity into 0, and filling the holes inside the body in the binary image; (e) using the region-growing algorithm to extract the body boundary by growing from the seed point; (f) Due to the well-defined natural contrast of the liver and lung, the boundary of diaphragm is clear and accurate in the two boundaries obtained in steps (c) and (e). taking the overlap part of these two boundaries to extract the diaphragm structure; (g) extracting the diaphragm from next sagittal slice by using the centroid of the grown-region in step (c) as the seed point of next iteration to make the process more automated. The 10 diaphragm structures extracted from the sagittal images that represent 10 different respiratory bins are used in later steps to guide the sorting process of axial slices. The diaphragm positions in axial slices are extracted by a peak-valley detection algorithm. The profiles of the intersection line of each axial image and single-slice cine image (Yellow dash line in Fig. 1) are analyzed by a peak-valley detection program to find the boundary point of liver and lung due to the naturally defined contrast of liver and lung. The peak-valley detection program is developed in Matlab (MathWorks, Natick, MA) to find true peaks and valleys in the image line profile by ignoring small local fluctuations caused by imaging noise.

(3) Sorting by diaphragm matching reference sagittal images to axial images: The sorting process is performed by matching the diaphragm position in the axial images with the 10 reference diaphragm structures extracted from sagittal images and then sort the

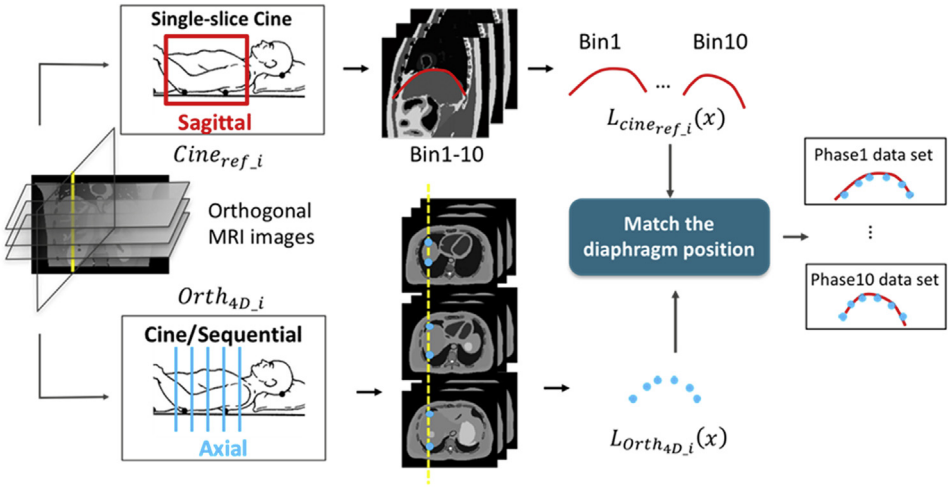

Fig. 1. The overall workflow of the anatomic feature matching-based 4D-MRI sorting method.

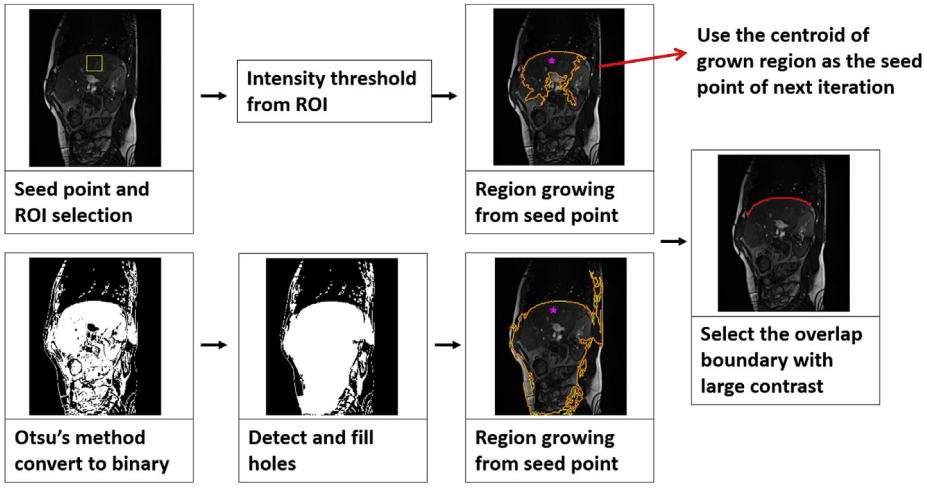

Fig. 2. The workflow of extracting diaphragm structures from the sagittal cine MRI images.

axial images into the corresponding phase bins. The diaphragm boundary extracted from the sagittal reference images can be described as $L_{ref_i}(x)$, where i represents the phase bin 1-10. The boundary from the axial slices can be represented as $L_{axial_{4D\_i}}(x)$. The sorting process to get the 3D volume of phase i (which is $4D\_i$) can be considered as finding the axial slice set that can minimize the difference between $L_{axial_{4D\_i}}(x)$ and $L_{ref_i}(x)$. This process can be expressed as:

$$Diff = \sum_{x=1}^{N} \left| L_{axial_{4D\_i}}(x) - L_{ref_i}(x) \right| \tag{1}$$

$$4D\_i = argmin\left(Diff\left(L_{axial_{4D\_i}}(x), L_{ref_i}(x) \right) \right) \tag{2}$$

2.1.2. Strategy for sorting slices outside the diaphragm region

The beginning and ending slices in the axial MRI scan may not contain diaphragm structures. The diaphragm matching method is then combined with other sorting methods to assign those slices into their corresponding bins. In this method, these out-of-diaphragm images are sorted based on the maximum cross-correlation (CC) of the profiles in the sagittal/axial images at the sagittal-axial intersecting plane. The cross-correlation can be defined as the formula below:

$$CC = \frac{E((x-\bar{x})(y-\bar{y}))}{\sigma_x \sigma_y} \tag{3}$$

where the x represents the pixels of the profile in sagittal image and y represents the pixels of the profile in axial image. E represents the expectation and σ means the standard deviation.

For example, an out-of-diaphragm axial slice can be assigned into phase bin N when:

$$\max\left(CC_{sagi_1}, \ldots, CC_{sagi_{10}} \right) = CC_{sagi_N} \tag{4}$$

where CC_{sagi_i} means the cross correlation between the axial profile and the sagittal profile of phase i.

2.1.3. Strategy for sorting slices outside the diaphragm region

Following the sorting process, each axial slice can be assigned to a certain phase bin corresponding to the diaphragm position. However, there might be empty bins for a certain phase at certain slice location. To solve this problem, a strategy is implemented to first copy the same slice from the phase in opposite slope. If that phase bin is also empty, then copy the slice from adjacent slices in the same phase. If the previous bins are empty, copy the same slice from adjacent phases. In addition, there might be bins for a certain slice location at a certain phase that are overfilled with multiple images. To solve this situation, another strategy is implemented to keep the slice which has the largest sagittal-axial intersecting profile cross correlation of the corresponding phase. After every slice bin of each phase is filled with only one image, then the ten 3D volumes are reconstructed by combining the axial slices together, and then further reconstructing a 4D volume.

2.1.4. Phase sorting

The conventional phase sorting method is also applied in every simulation case to further compare with the anatomic feature matching methods [26]. For a known breathing signal, a peak/valley detection is performed to detect every breathing peak during a scan. The interval between two neighboring peaks is regarded as a single respiratory cycle and then is divided into 10 equally-spaced bins. Each image will be assigned into a phase bin if its acquisition time stamp falls into the corresponding bin in that cycle. The strategy for empty phase bins is the same as the anatomic feature matching method. However, for the redundant images in one phase bin, the image acquired at the closest time point to the bin center is kept.

2.2. Digital phantom simulation study

2.2.1. Materials

This 4D-MRI sorting technique was developed and evaluated using the 4D extended Cardiac Torso (XCAT) digital phantom to simulate the image acquisition and reconstruction.[16] The XCAT images were created in the activity mode with organs' intensities assigned as in T2-weighted MR images. The liver lesion is set to be 30 mm in diameter and to move with liver together during respiration. The respiratory motion of the XCAT digital phantom is controlled by the input breathing signals.

2.2.2. Breathing simulation

The effects of breathing signals, including both regular and irregular in both axial cine and sequential modes, are simulated and investigated. First, cine and sequential scans are simulated with a regular cosine breathing pattern in XCAT digital phantom. The parameters of the simulated images are set to mimic the real MRI scan: voxel size: 1.67 × 1.67 × 1.67 mm^3; frame rate: 0.3 s/frame; respiratory rate: 3.1 s/cycle; maximum diaphragm displacement: 3 cm.

Secondly, cine and sequential scans with three types of irregular breathing profiles are simulated in the XCAT digital phantom. The parameters of the simulated images are set to mimic the real MRI scan: voxel size: 1.67 × 1.67 × 5.00 mm^3; frame rate: 0.3 s/frame; maximum diaphragm displacement: 3 cm. Three types of irregular breathing

profiles are simulated based on simple cosine signal as is shown in Fig. 3: (a) cosine signal with changing periods; (b) cosine signal with changing amplitudes; and (c) cosine signal with changing periods and amplitudes. In addition, five patients' breathing signals acquired with the Real-time Position Management (RPM) system (Varian Medical Systems, Palo Alto, CA) are used to simulate the cine and sequential scans in the XCAT digital phantom. As is shown in Fig. 4, these signals are preprocessed to remove some extreme peaks and valleys before using for scan simulation.

2.3. Assessment

Three metrics were implemented to further evaluate the performance of this anatomic matching based sorting method regarding its volumetric accuracies of both whole 4D image and tumor.

Total relative error (TRE) measures the relative difference between the reconstructed image and the ground truth image over the whole 4D volume. If two images are identical, the TRE will be 1. TRE can be calculated by the formula below:

$$TRE = \frac{\sqrt{(f - f_{GT})^2}}{\sqrt{f_{GT}^2}} \times 100\% \quad (5)$$

where f is the reconstructed 4D image and f_{GT} is the ground truth image.

Tumors in the images were automatically contoured using an in-house developed Matlab program. Then the Volume-Percent-Difference (VPD) metric is utilized to estimate the accuracy of tumor volume in the 4D images compared with the ground truth images. VPD was calculated using the formula below:

$$VPD = \frac{|V \cup V_0 - V \cap V_0|}{V_0} \times 100\% \quad (6)$$

where V_0 is the tumor volume in the ground truth image and V is the tumor volume in the reconstructed 4D images. VPD will be 0 if the two 4D images sets are identical.

Center-of-Mass-Shift (COMS) represents the shift of the tumor center;

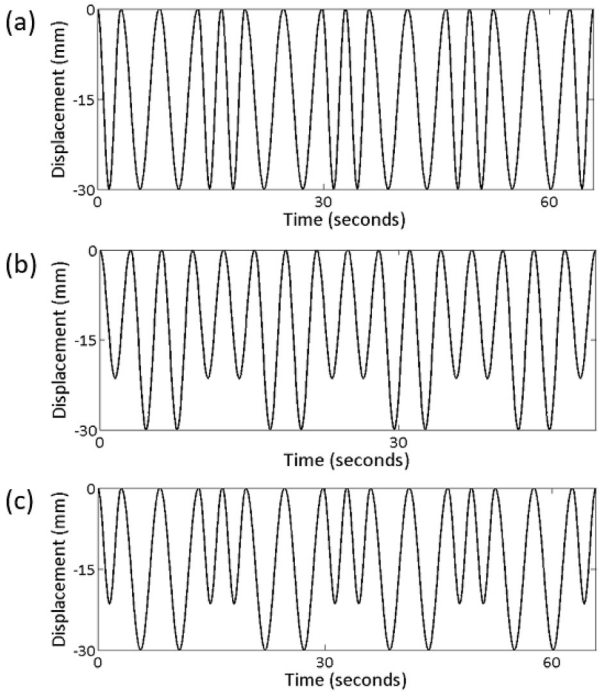

Fig. 3. Simulated irregular breathing curves used for raw MRI data simulation: (a) cosine curve with changing period; (b) cosine curve with changing amplitude; and (c) cosine curve with changing period and amplitude.

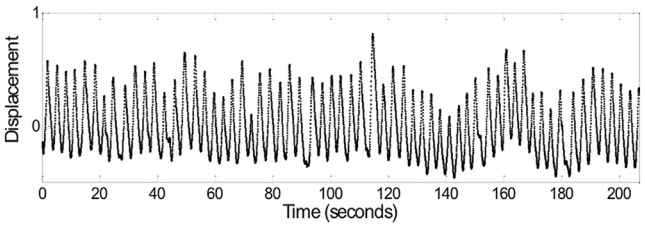

Fig. 4. One example of the patient breathing curves used for raw MRI data simulation. The patient breathing signal is acquired by the RPM system.

ideally it is 1 when the reconstructed image perfectly is matched with the ground truth. It was estimated using the formula below:

$$COMS = \sqrt{\Delta x^2 + \Delta y^2 + \Delta z^2} \quad (7)$$

where Δx, Δy and Δx is the center-of-mass distance from the tumor volume in 4D image to the tumor in the ground truth.

3. Results

Fig. 5 shows the result of the 4D images generated by the anatomic feature matching-based method, as compared to the conventional phase sorting (Phase S) method and the ground truth images in both cine and sequential acquisition modes with a regular cosine breathing pattern. The subtraction of the reconstructed 4D images by anatomic feature matching from the ground truth (GT) images, or the difference maps, are also generated for better visual evaluation. Only first five phases of the 4D image set including the end of exhalation (EOE) and end of inhalation (EOI) phases are displayed in the figure. In the difference map (5d), it can be found that the reconstructed images from the anatomic feature matching method matched well with the ground truth images with minimal artifacts. In the 30% phase bin, artifacts are visible in the heart region, which are indicated by the blue arrows. These artifacts are caused by the difference between the nonsynchronous periods of heart motion and respiratory motion, which is not the major consideration of this study. In the red box in Fig. 5, it can be observed that the images generated by anatomic feature matching method can preserve a clear and smooth diaphragm structure, while the diaphragm boundary is blurred in the phase sorting method. The red arrows in Fig. 5 also indicate the tumor volume comparison. The result of both cine and sequential acquisitions showed good consistency with the ground truth.

Fig. 6 shows the reconstruction results of the anatomic feature based on matching-based sorting method using one example simulated cosine-based irregular signal with changing period and amplitude, compared with the conventional phase sorting method (6b, 6e) and the ground truth images (6c, 6f) in both cine and sequential acquisition modes. Fig. 7 shows the reconstruction results based on the anatomic feature matching-based sorting method using one example patient irregular breathing signal compared with the conventional phase sorting method and the ground truth images in both cine and sequential acquisition modes. As is indicated in the difference maps between the sorted images and the ground truth, the anatomic feature matching-based sorting method can generate 4D MRI images with minimal artifacts. Compared with the results of conventional phase sorting, this method can provide better anatomic structure consistency. It can be found from the red boxes and red arrows in the figures that the artifacts in the phase sorting result are more obvious as truncated diaphragm boundary and distorted tumor shapes compared with the proposed method. This improvement made by the anatomic feature matching method is strengthened with larger irregularity of the breathing pattern, which can be observed by comparing the results in Figs. 6 and 7. In addition, both the cine and sequential acquisition modes showed promising results with the anatomic feature matching-based 4D-MRI sorting method in irregular breathing.

Table 1 shows the quantitative evaluation of the anatomic feature

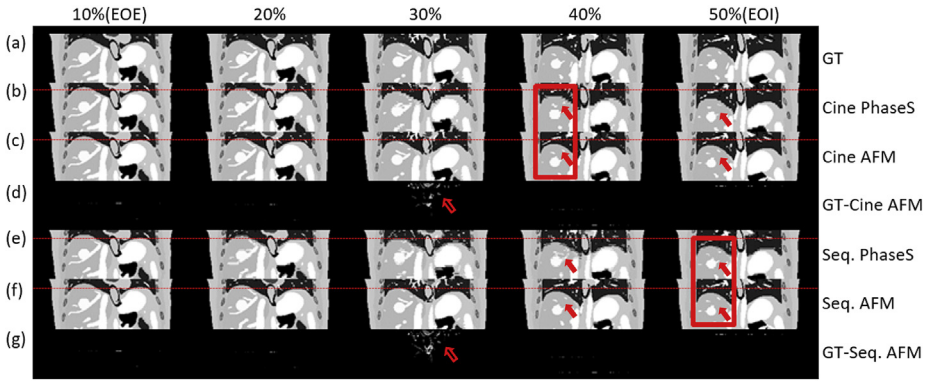

Fig. 5. For regular breathing pattern: (a) The ground truth 4D image in first 5 phases. (b) 5-phase phase sorting result of cine acquisition. (c) 5-phase anatomic feature matching-based sorting result of cine acquisition. (d) Difference map between the ground truth and the anatomic feature matching-based sorting result in cine mode. (e) 5-phase phase sorting result of sequential acquisition. (f) 5-phase anatomic feature matching-based sorting result of sequential acquisition. (g) Difference map between the ground truth and the anatomic feature matching-based sorting result in sequential mode.

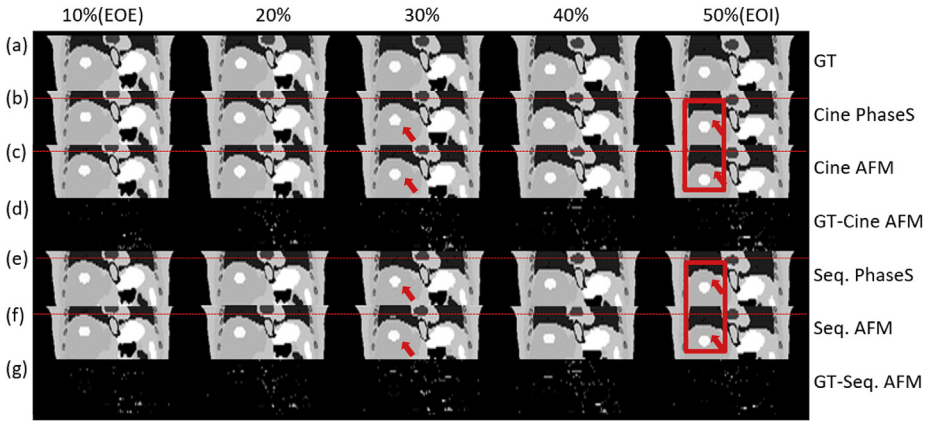

Fig. 6. For simulated irregular breathing with changing period and amplitude: (a) The ground truth 4D image in first 5 phases. (b) 5-phase phase sorting result of cine acquisition. (c) 5-phase anatomic feature matching-based sorting result of cine acquisition. (d) Difference map between the ground truth and the anatomic feature matching-based sorting result in cine mode. (e) 5-phase phase sorting result of sequential acquisition. (f) 5-phase anatomic feature matching-based sorting result of sequential acquisition. (g) Difference map between the ground truth and the anatomic feature matching-based sorting result in sequential mode.

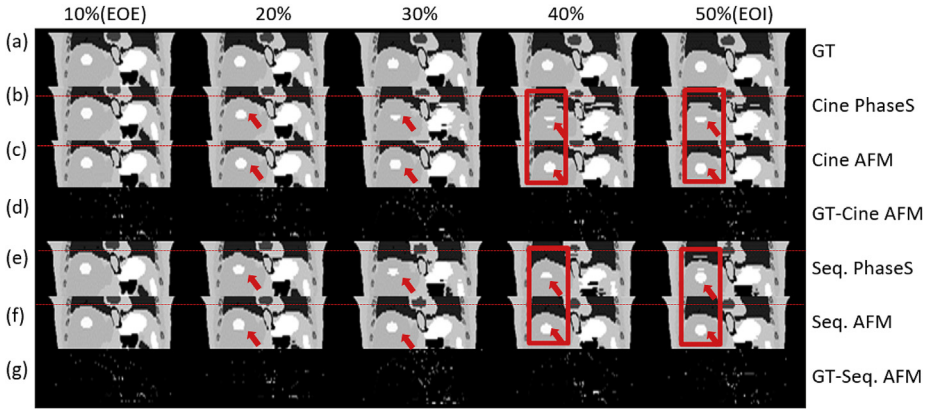

Fig. 7. For patient irregular breathing signal #1: (a) The ground truth 4D image in first 5 phases. (b) 5-phase phase sorting result of cine acquisition. (c) 5-phase anatomic feature matching-based sorting result of cine acquisition. (d) Difference map between the ground truth and the anatomic feature matching-based sorting result in cine mode. (e) 5-phase phase sorting result of sequential acquisition. (f) 5-phase anatomic feature matching-based sorting result of sequential acquisition. (g) Difference map between the ground truth and the anatomic feature matching-based sorting result in sequential mode.

Table 1
Regular breathing evaluation results using three different metrics.

Case	TRE	VPD	COMS
Cine	0.28%	1.16%	0.06 mm
Sequential	0.35%	1.23%	0.04 mm
Mean_AFM	0.32%	1.20%	0.05 mm
Mean_PhaseS	0.77%	1.87%	0.10 mm

matching-based sorting method for both cine and sequential acquisition in regular breathing pattern, regarding the accuracy of whole 4D image volume and the estimated tumor volume in the 4D images. It can be indicated from this table that this anatomic feature matching-based sorting method can provide good tumor volume consistency on average with minimal 4D volume difference with the ground truth. Both cine and sequential modes can reconstruct 4D-MRI images with improved accuracy and clear organ/tissue structures with minimum mismatch.

Table 2 and Table 3 show the quantitative evaluation of the anatomic feature matching-based sorting method compared with the conventional phase sorting method for both cine and sequential acquisition in irregular breathing patterns, including simulated and patient breathing respectively, regarding the accuracy of whole 4D image volume intensity and the estimated tumor volume in the 4D images. It can be found from these tables that the anatomic featuring matching-based 4D-MRI sorting method can provide accurate volumetric information about the tumor and body compared with the conventional phase sorting results. The minimal values of TRE, VPD and COMS for this proposed method can indicate the reduced motion artifacts regarding the image quality.

Table 2
Simulated irregular breathing result evaluation.

Case#		TRE	VPD	COMS
Cine	Prd	0.79%	4.19%	0.19 mm
	Amp	1.09%	4.98%	0.21 mm
	PrdAmp	0.93%	6.51%	0.31 mm
	Mean	0.93%	5.23%	0.24 mm
Seq.	Prd	1.22%	4.91%	0.30 mm
	Amp	1.39%	5.93%	0.31 mm
	PrdAmp	1.39%	7.37%	0.36 mm
	Mean	1.33%	6.07%	0.32 mm
Mean_AFM		1.02%	5.65%	0.28 mm
Mean_PhaseS		1.13%	10.47%	0.49 mm

Note: Prd: the cosine-based breathing signal is changing in period only. Amp: the cosine-based breathing signal is changing amplitude only. PrdAmp: the cosine-based breathing signal is changing in both period and amplitude.

Table 3
Patient irregular breathing result evaluation.

Case#		TRE	VPD	COMS
Cine	1	0.97%	6.05%	0.50 mm
	2	1.09%	5.89%	0.25 mm
	3	1.26%	9.91%	0.36 mm
	4	0.93%	5.37%	0.23 mm
	5	1.03%	7.90%	0.28 mm
	Mean	1.06%	7.02%	0.32 mm
Seq.	1	1.10%	5.52%	0.10 mm
	2	1.13%	8.05%	0.15 mm
	3	1.27%	8.54%	0.53 mm
	4	1.37%	7.58%	0.14 mm
	5	1.17%	7.10%	0.18 mm
	Mean	1.21%	7.36%	0.42 mm
Mean_AFM		1.13%	4.26%	0.37 mm
Mean_PhaseS		2.97%	25.85%	1.23 mm

Besides, the values for the cine acquisition and sequential acquisition are very close in the implement of two different kinds of irregular breathing signals, which shows the feasibility of this sorting method in both MRI acquisition modes.

4. Discussion

Breathing variation related artifacts are inherent in the conventional 4D MRI images, which can be shown as discontinuities in the organ structures. Different approaches have been developed to reduce this motion artifact. For instance, Hu et al.[11] developed a prospective 4D-MRI technique to implement an amplitude-based gating system to avoid the imaging during the irregular breathing patterns. Liang et al.[17] developed a retrospective 4D-MRI sorting method as probability-based multi-cycle sorting to incorporate breathing variation information in the sorting process to reduce the related artifacts. But due to the sorting scheme, this probability-based multi-cycle sorting cannot be applied in cine acquisition, which will limit the choices of imaging sequences and the related contrast selection.

In this study, a robust 4D-MRI sorting method based on anatomic feature matching was developed and investigated to largely reduce the breathing variation related artifacts due to another new approach, which is to directly preserve the organ/tissue structures by aligning or matching them in two group of orthogonal images. The methods mentioned above utilized external breathing signals to guide the sorting or reconstruction procedure, which requires additional synchronization and correlation of the scan and breathing signal. This new method utilized the change of anatomic feature in images to form the bins and to guide the sorting process, which can provide better validity and accuracy. In addition, some of the previous methods are only applicable in a specific data acquisition mode. However, for the anatomic feature matching method, it is feasible in both cine and sequential mode, which enables a wider choice of imaging sequences and contrasts.

As is shown in the results, the reconstructed 4D-MRI images are in great consistency with the ground truth and show substantially reduced motion artifacts and clearer organ structures compared with the conventional phase sorting method. This is more obvious in the patient breathing case, where the anatomic feature matching-based sorting method can still generate images with smooth organ structures and minimal artifacts, while the irregular breathing pattern strongly influences the performance of phase sorting method. The artifacts are more likely to be found in the EOI phase in the reconstructed images, while the EOE phase images show better consistency with the ground truth. This is consistent with the fact that EOI is the less stable phase in a breathing cycle and EOE is the more stable phase. It can also be found from the quantitative analysis that this new sorting method can provide good overall volumetric accuracy with only 1.13% total relative error, and as small as 7.19% volume difference and 0.37 mm center-of-mass shift for the target volume, which is greatly improved compared with the conventional method.

In addition, from Tables 1–3 it can be found that the result of cine acquisition provides slightly better consistency with the ground truth than the result of the sequential acquisition. This is potentially due to the different scanning strategies of these two scan modes. All the simulated scans have the same number of scan repetitions; that is, 20 times. For the cine acquisition, it continuously obtains images at one slice position over several breathing cycles to provide continuous diaphragm motion. However, for the sequential acquisition which acquire images slice location by slice location, this process is more random, and it is harder to predict the completeness for the slices to fill all the phase bins.

First of all, this 4D-MRI sorting method based on anatomic feature matching is tested only on the XCAT digital phantom. Only 5 clinical patient breathing signals were utilized to simulate the raw MRI data. Further investigation using more patient breathing signals is needed to study the significance of this new sorting method. Besides, only the diaphragm extraction part has been practiced on real patient images so far. The performance of this method in patient image data needs to be further tested to evaluate its robustness and accuracy in different patient scenarios.

The patient breathing data used in this study was preprocessed to eliminate some extreme peaks and valleys that might be caused by coughing or other large motion during the acquisition. Thus, the simulation process only simulates images under free breathing without extreme irregularity. Since the 2D images are sorted by matching anatomic feature from the images of an averaged breathing curve. The presence of coughing and large motion can cause insufficient useful data and might further result in empty phase bins. The influence of the extreme irregularity can be investigated by adding large peaks and valleys in the breathing signal in simulation.

In addition, the current diaphragm extraction methods still need manual operation in the very first step. It needs to be further automated to improve the robustness and operation speed, with a goal of full automation. The simulated MRI images generated from XCAT have good pixel intensity contrast, which makes the diaphragm extraction less sensitive to the noise and resolution limitation. Therefore, this extraction method need to be further improved to provide more accurate results in the patient image, which has higher noise and more complicated pixel intensity shifts.

Another limitation of this study is that this sorting method can only work for the axial slices which contain the diaphragm structure. For real patient data with larger slice thickness, the number of slice positions that meets this requirement might be limited. Smaller slice thickness allows more slices within the diaphragm region, but can be more sensitive to the breathing irregularity, and it needs more time in the acquisition. Larger slices thickness can shorten the acquisition time and make the sorting process less sensitive to the irregularity, however, it will limit the resolution and number of slices to cover the diaphragm. In this study, the slice thickness is set as 0.5 cm, which is common in the 4D-MRI scans. To sort

other axial slices outside the diaphragm region, this method needs to be hybridized with other 4D-MRI sorting methods, or to utilize other anatomic features to generate the 4D-MRI volume for the whole abdominal region. Other possible anatomic landmarks like the body surface, lung boundary and other large-contrast edges may be investigated in the future to test the feasibility.

5. Conclusion

A 4D-MRI technique based on anatomic feature matching method has been developed and evaluated in a digital phantom. It utilizes the diaphragm structure as the landmark feature in two groups of orthogonal images to guide the sorting process. This anatomic feature matching-based method is feasible and can be applied in both cine and sequential acquisition modes. In addition, it is less susceptible to breathing variations and can generate 4D-MRI images with significantly reduced motion artifacts.

Conflict of Interest

None.

Acknowledgement

This research was partly supported by research grants (NIH R01 EB028324, NIH R01 CA226899, GRF 151021/18M, GRF 151022/19M and HMRF 06173276).

References

1. Keall P. 4-dimensional computed tomography imaging and treatment planning. *Semin Radiat Oncol.* 2004;14:81–90.
2. Low DA, Nystrom M, Kalinin E, et al. A method for the reconstruction of four-dimensional synchronized CT scans acquired during free breathing. *Med Phys.* 2003; 30:1254–1263.
3. Liu Y, Yin FF, Czito BG, Bashir MR, Cai J. T2-weighted four dimensional magnetic resonance imaging with result-driven phase sorting. *Med Phys.* 2015;42:4460–4471.
4. Cai J, Chang Z, Wang Z, Paul Segars W, Yin FF. Four-dimensional magnetic resonance imaging (4D-MRI) using image-based respiratory surrogate: a feasibility study. *Med Phys.* 2011;38:6384–6394.
5. Wang C, Subashi E, Yin FF, Chang Z, Cai J. A spatiotemporal-constrained sorting method for motion-robust 4D-MRI: a feasibility study. *Int J Radiat Oncol Biol Phys.* 2019;103:758–766.
6. Dinkel J, Hintze C, Tetzlaff R, et al. 4D-MRI analysis of lung tumor motion in patients with hemidiaphragmatic paralysis. *Radiother Oncol.* 2009;91:449–454.
7. von Siebenthal M, Szekely G, Gamper U, Boesiger P, Lomax A, Cattin P. 4D MR imaging of respiratory organ motion and its variability. *Phys Med Biol.* 2007;52: 1547–1564.
8. Remmert G, Biederer J, Lohberger F, Fabel M, Hartmann GH. Four-dimensional magnetic resonance imaging for the determination of tumour movement and its evaluation using a dynamic porcine lung phantom. *Phys Med Biol.* 2007;52: N401–N415.
9. Liu Y, Zhong X, Czito BG, et al. Four-dimensional diffusion-weighted MR imaging (4D-DWI): a feasibility study. *Med Phys.* 2017;44:397–406.
10. Liu Y, Yin FF, Chen NK, Chu ML, Cai J. Four dimensional magnetic resonance imaging with retrospective k-space reordering: a feasibility study. *Med Phys.* 2015; 42:534–541.
11. Hu Y, Caruthers SD, Low DA, Parikh PJ, Mutic S. Respiratory amplitude guided 4-dimensional magnetic resonance imaging. *Int J Radiat Oncol Biol Phys.* 2013;86: 198–204.
12. Deng Z, Pang J, Yang W, et al. Four-dimensional MRI using three-dimensional radial sampling with respiratory self-gating to characterize temporal phase-resolved respiratory motion in the abdomen. *Magn Reson Med.* 2016;75:1574–1585.
13. Stemkens B, Paulson ES, Tijssen RHN. Nuts and bolts of 4D-MRI for radiotherapy. *Phys Med Biol.* 2018;63:21TR01.
14. Lee D, Greer PB, Paganelli C, Ludbrook JJ, Kim T, Keall P. Audiovisual biofeedback improves the correlation between internal/external surrogate motion and lung tumor motion. *Med Phys.* 2018;45:1009–1017.
15. Otsu N. A threshold selection method from gray-level histograms. *IEEE Trans Syst Man Cybern.* 2016:62–66, 19799.
16. Segars WP, Tsui BMW, Cai J, Yin FF, Fung GSK, Samei E. *Application of the 4-D XCAT Phantoms in Biomedical Imaging and Beyond.* vol. 37. 2018:680–692, 3.
17. Liang X, Yin FF, Liu Y, Cai J. A probability-based multi-cycle sorting method for 4D-MRI: a simulation study. *Med Phys.* 2016;43:6375–6385.